This article has been accepted for publication in a future issue of this journal, but has not been fully edited. Content may change prior to final publication. Citation information: DOI 10.1109/TPWRS.2020.2999488, IEEE Transactions on Power Systems

Event-Triggered Load Frequency Control via Switching Approach

Sahaj Saxena, Member, IEEE, and Emilia Fridman, Fellow, IEEE,

Abstract—Event-triggered control (ETC) is becoming increasingly popular in load frequency control (LFC) operation in power systems. So far, the existing literature has primarily focused on load disturbance rejection in face of communication delay without considering much on networked-induced measurement disturbances and messages sent. In this paper, we study the LFC operation as a problem of networked control system and propose, for the first time, an ETC based switching approach for frequency regulation. We derive delay-dependent conditions to obtain the lower bound on inter-event time during event-trigger mechanism which assures the robust stability under networked induced time-varying delays and measurement disturbance and reduction in the amount of sent measurements. The effectiveness of the proposed approach is verified via numerical examples based on single-, two-area power systems and single-area with electric vehicle (EV) participation.

Index Terms—Event-triggered control, electric vehicles, PI control, periodic sampling, time-delays.

I. Introduction

THE study of time-delay has aroused wide interest in LFC operation of power systems due to (i) existence of geographically distributed generators and load, (ii) usage of more open, adaptable and distributed communication network infrastructure, and (iii) increased competition among third party or bilateral contracts in offering better ancillary services. In addition to the delay in control signal, intrusion of communication noises and malicious signal breaching (cyber-attack) are also important issues [1]–[4]. Ignoring these phenomenon in network dynamics may lead to failure or inappropriate functioning of existing LFC approaches (e.g., [5]–[8]). Thus it is essential to consider time-delays and disturbances.

In the past two decades, substantial research has been done to ensure the stable LFC operation under time-delayed communication. In face of delayed control signal, the LFC study conducted in [9] and [10] presented the idea of determining a delay bound and LMI-based robust control theory. Later on, this approach is generalized by using Lyapunov–Krasovskii functional (LKF) [11] for stability and stabilization of LFC processes to overcome the effect of time-delays [12]. Specifically, an improved weighing matrix approach is used to devise a delay-dependent bounded real lemma [13] for analysis. A new delay-dependent LMI criterion based on Park's inequality [14] and truncated infinite series integral inequality [15] and Bessel–Legendre inequality [16] were also proposed. An LMI-based robust predictive control state-feedback law was designed in [17]. A new free weighing matrix with a refined Jensen inequality based stability condition was suggested for EV supported LFC operation [18]. Recently a unified approach of fuzzy H_∞ and iterative learning was suggested in [19] for time-varying communication delays. In addition to it, different delay-dependent stability conditions using delay margin for LFC systems have been studied in [20], [21] and references therein. However, the explicit treatment of communication constraints (uncertain fast-varying time-delays, external disturbance) in the networked-power systems during LFC operation is still a difficult task.

Another challenge for large-scale power systems operating in distributed network communication system is the implementation of LFC mechanism under heavy transmission burden and brief communication times via band-limited channel. The ETC algorithm serves as a suitable candidate for reduction of communication burden between sensors, controller and actuator nodes (see [22] and references therein). Consequently, the LFC schemes augmenting the ETC approaches via proportional-integral (PI) control [23], sliding mode control [24], supplementary adaptive dynamic programming controller [25], observer-based controller [26] were proposed for time-delayed power systems. An adaptive ETC strategy (opposite to the fixed threshold parameter to fulfill event-triggering condition) was also proposed to reduce the number of transmissions [27].

The comprehensive survey, thus far, signifies that ETC approaches and LKF-based stability conditions represent a promising framework for efficient LFC operation. Besides solutions to time variations in practical power network (due to message losses, link failure, etc.), the explicit considerations of communication uncertainties due to channel disturbance and cyber-attack are still required. Congestion control and channel quality enhancement by transmitting the reduced amount of measurement signals is still an open problem in networked power systems. Keeping these issues in mind, we aim to achieve robust and stable networked-control LFC operation. We summarize our contribution in the following paragraph.

This paper addresses the LFC operation of power

This work was supported by Israel Science Foundation (grant no. 673/19) and by Thapar Institute of Engineering and Technology.

Sahaj Saxena is with the School of Electrical Engineering, Tel Aviv University, Israel, and also with the Electrical and Instrumentation Engineering Department, Thapar Institute of Engineering and Technology, Patiala, India (e-mail: sahajsaxena11@gmail.com).

Emilia Fridman is with the School of Electrical Engineering, Tel Aviv University, Israel (e-mail: emilia@tauex.tau.ac.il).

0885-8950 (c) 2020 IEEE. Personal use is permitted, but republication/redistribution requires IEEE permission. See http://www.ieee.org/publications_standards/publications/rights/index.html for more information.
Authorized licensed use limited to: TEL AVIV UNIVERSITY. Downloaded on June 06,2020 at 10:31:27 UTC from IEEE Xplore. Restrictions apply.

This article has been accepted for publication in a future issue of this journal, but has not been fully edited. Content may change prior to final publication. Citation information: DOI 10.1109/TPWRS.2020.2999488, IEEE Transactions on Power Systems

system under networked control framework where sampled in time measurements are transmitted through communication network having uncertainties of time-delays and network induced disturbances. Unlike the conventional discrete time control which employs periodic sampling of measurements (thereby creating redundancy), we consider a continuous event-triggering (ET) mechanism but with certain waiting time, i.e., whenever the ET condition gets violated, the measurement is sent and then the ET mechanism waits for some time and then restarts its operation. We adopted this approach of [28] under PI control strategy and proposed a new resource aware LFC approach which reduces the amount of sent measurement by switching between periodic sampling and continuous ET. Our idea is to wait for at least certain time interval at sensor end when frequency measurements are sent. This waiting time is derived using delay-dependent stability condition via LMI tool and LKF. After waiting, the sensor continuously monitor the ET condition and release measurements when it is violated. We demonstrate that this approach (i) reduces redundant transmission of packets which arises due to periodic sampling, (ii) avoids Zeno phenomenon which occurs due to continuous ET, (iii) yields larger inter-sampling time interval for same ET conditions,and (iv) guarantees the desired L_2-gain (within the prescribed value) of the closed-loop system. Thus, the overall workload is minimized during LFC operation. To illustrate the effectiveness of derived approach, we study the single- and two-area power systems under networked induced uncertain time-varying delays, and measurement and load disturbances. We also employed the approach to a deregulated system where the EV takes part in power generation. For comparative study, we applied the periodic sampling and periodic ET schemes and it is observed that the switching approach requires less amount of measurements in comparison to the former schemes in all the cases. Moreover, the waiting time is also larger than the periodic ET approach.

The rest of the paper is organized as follows. We formulate the LFC operation of the single-area power system in Section II and introduce the switching approach in Section III. This approach is sequentially extended to two-area and single-area power systems with EV participation in Sections IV and V, respectively. Simulation results of power system under different configuration are presented in Section VI. Brief summary and outlook for future research are described in Section VII.

Notations: We define the sets $\mathbb{R}$ and $\mathbb{N}$ a set of real and natural numbers, respectively. Let $x = \text{col}\{x_i\} \in \mathbb{R}^n$ denote a vector with entries x_i for $i \in 1, ..., n$. For $A \in \mathbb{R}^{n\times n}, A > 0$ means A is symmetric positive definite matrix. We denote by $L_2[0,\infty]$, the space of function $f : [0,\infty) \to \mathbb{R}^n$ with the norm $||f||_{L_2} = [\int_0^\infty |f(\phi)|d\phi]^{1/2} < \infty$ where $|f(\cdot)|$ is the standard Euclidean norm on $\mathbb{R}^n$.

II. Problem set-up for single-area LFC

Power systems are generally nonlinear. However linearized models are acceptable in LFC problems because the load has very small fluctuations. Following [17], [29], [30], we study a standard simplified power generator network comprising of governor, non-reheated turbine, and load and machine (see Fig. 1). The units in control area are assumed to be coherent and in order to obtain the area frequency deviation $\Delta f(t)$, the generators are lumped. The models of generator and load, turbine and governor dynamics are given by [29]:

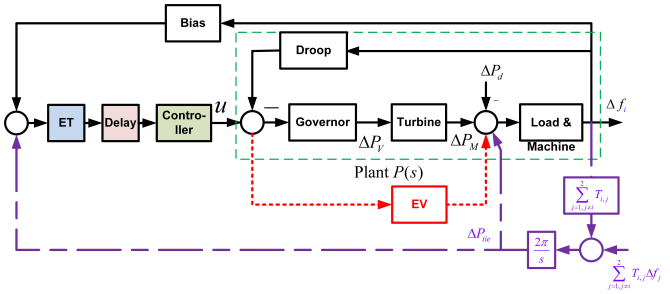

Fig. 1: Dynamic model of control area. Power system within green block (–) represents single-area configuration. Green Block together with magenta (– -) blocks depicts ith area and green and red blocks $(\cdots)$ together describes the control-area supported with electric vehicle.

$$\Delta\dot{f}(t) = -\frac{D}{M}\Delta f(t) + \frac{1}{M}\Delta P_M(t) - \frac{1}{M}\Delta P_d(t), \quad (1a)$$

$$\Delta\dot{P}_M(t) = -\frac{1}{T_T}\Delta P_M(t) + \frac{1}{T_T}\Delta P_V(t), \quad (1b)$$

$$\Delta\dot{P}_V(t) = -\frac{1}{T_G}\Delta P_V(t) - \frac{1}{RT_G}\Delta f(t) + \alpha_G\frac{1}{T_G}u(t), \quad (1c)$$

where T_G, M, T_T, D, R denote the governor time constant, generator inertia constant, turbine time constant, damping coefficient, and droop constant, respectively. The parameter α_G is a participation factor for LFC which is set to unity in absence of other generation unit. The variables ΔP_V, ΔP_M and ΔP_d denote the deviation in valve position, generator mechanical output, and load, respectively. Finally, $u \in \mathbb{R}$ is a control input.

We assume that the load disturbance $\Delta P_d(t)$ satisfies $\Delta P_d(t) \in L_2[0,\infty]$ and there exists a synchronous (steady-state) solution to the power system model (1). This is required for the existence of desired control signal which can drive the system to predefined state. We present the Lemma II.1 to elaborate the synchronous solution. Our proof is along the lines of [31, Lemma 1].

Lemma II.1. Given the synchronous (steady-state) solution $(\Delta f, \Delta P_M, \Delta P_V)$ of (1), the synchronous (steady-state) frequency deviation is given by

$$\Delta f^*(t) = \frac{-\Delta P_d(t) + u^*(t)}{-D - R^{-1}} \quad (2)$$

where $u^*(t)$ denotes the steady-state control action.

Proof. In synchronized state, (1b) reduces to $\Delta P_M(t) = \Delta P_V(t)$ and (1c) to $\Delta P_V(t) = u(t) - \frac{\Delta f(t)}{R}$ and subsequently (1a) gives $-(D + R^{-1})\Delta f(t) + u(t) - \Delta P_d(t) = 0$ and we arrive at (2). □

0885-8950 (c) 2020 IEEE. Personal use is permitted, but republication/redistribution requires IEEE permission. See http://www.ieee.org/publications_standards/publications/rights/index.html for more information.
Authorized licensed use limited to: TEL AVIV UNIVERSITY. Downloaded on June 06,2020 at 10:31:27 UTC from IEEE Xplore. Restrictions apply.

This article has been accepted for publication in a future issue of this journal, but has not been fully edited. Content may change prior to final publication. Citation information: DOI 10.1109/TPWRS.2020.2999488, IEEE Transactions on Power Systems

Note that in (2), if $\Delta f^*(t) = 0$ then $-\Delta P_d + u^* = 0$ and we achieve a balance between generation and demand. In this case, a synchronous solution is of the form $(\Delta f^*, \Delta P_M^*, \Delta P_V^*, u^*) = (0, 0, 0, \mathcal{U})$ where $\mathcal{U} \in \mathbb{R}$. Therefore, our main objective is regulation of frequency deviation and Δf converges asymptotically to zero, i.e.,

$$\lim_{t\to 0}\Delta f(t) = 0 \ \forall \Delta P_d. \tag{3}$$

In LFC operation, the area control error (ACE) ΔE is used to maintain zero steady-state error for frequency deviation, which is defined as

$$\Delta E(t) = \beta \Delta f(t), \tag{4}$$

where β is frequency bias constant. In order to stabilize frequency deviations, we employ a PI controller of the form

$$u(t) = -k_P \Delta E(t) - k_I \int_0^t \Delta E(t)dt, \tag{5}$$

where $k_P \in \mathbb{R}$ and $k_I \in \mathbb{R}$ are the proportional and integral gains, respectively. The PI controller offers a fast disturbance rejection response. Moreover, in absence of derivative term, it is immune to the effect of noise [32]. Note that the measurement y (namely the ΔE signal) can be affected by the network induced transmission (measurement) disturbance $v(t) \in L_2[0, \infty]$ and therefore, we have

$$y(t) = \begin{bmatrix} \beta \Delta f(t) + v(t) \\ \int_0^t \Delta E(t)dt \end{bmatrix}. \tag{6}$$

Under the representation (6), the controller (5) can now be transformed into a static output-feedback controller of the form

$$u(t) = -Ky(t), \tag{7}$$

where $K = [k_P, k_I]$.

Our contribution is to analyze the power system (1) for LFC operation in the framework of networked-based control system where we consider the sampled in time measurements $y(s_k)$ available at discrete time instants:

$$0 = s_0 < s_1 < s_2 < ..., \ \lim_{k\to\infty} s_k = \infty. \tag{8}$$

In such a scenario, the networked induced disturbance and uncertain time varying-delays may lead to instability of system.

Remark II.2. Network induced time-delays in power systems arise due to delay in telemeter signal (e.g., from remote terminal units to control center and control center to individual units, signal processing, control law updating), data packet dropout (which can be equivalently considered a time-varying delay [30]) and physical failures. Moreover, the constant time-delays signify a heavily congested network or a denial-of-service type attack whereas the random delays denote the Byzantine failures and malicious attacks [9].

Generally, the network induced unknown delays exist between sensor and actuator which can affect the transmission measurement $y(s_k)$. Therefore, in order to simplify the analysis, we assume that all such delays are combined into a single delay locating in forward loop (as depicted in Fig. 1) and is denoted by $\{\theta_k\}_{k\in\mathbb{N}} \leq \theta_M$, where θ_M is a known bound. Let s_k in (8) be sampling instants on the sensor side and the controller is implemented via zero-order hold (ZOH). Assuming θ_k in a manner that the ZOH updating times $t_k = s_k + \theta_k$ which satisfy [11], [33]

$$t_k = s_k + \theta_k \leq s_{k+1} + \theta_{k+1} = t_{k+1}, \quad k \in \mathbb{N} \tag{9}$$

then the controller (7) can be represented as

$$u(t) = Ky(s_k), \quad t \in [t_k, t_{k+1}). \tag{10}$$

Considering x=col$\{\Delta f, \Delta P_M, \Delta P_V, \int \Delta E\} \in \mathbb{R}^4$ as the augmented state vector, $z = \Delta f \in \mathbb{R}$ as the controlled output, and $\Delta P_d(t), v(t) \in \mathbb{R}$ as the load and measurement disturbances, we can represent the power system (1), (6) as

$$\dot{x}(t) = Ax(t) + Bu(t) + F\Delta P_d(t) \tag{11a}$$
$$z(t) = C_1 x(t) \tag{11b}$$
$$y(t) = C_2 x(t) + Dv(t) \tag{11c}$$

where

$$A = \begin{bmatrix} -\frac{D}{M} & \frac{1}{M} & 0 & 0 \\ 0 & -\frac{1}{T_T} & \frac{1}{T_T} & 0 \\ -\frac{1}{RT_G} & 0 & -\frac{1}{T_G} & 0 \\ \beta & 0 & 0 & 0 \end{bmatrix}, B = \begin{bmatrix} 0 \\ 0 \\ \frac{\alpha_G}{T_G} \\ 0 \end{bmatrix}, F = \begin{bmatrix} -\frac{1}{M} \\ 0 \\ 0 \\ 0 \end{bmatrix}$$
$$C_1 = [1\ 0\ 0\ 0], C_2 = \begin{bmatrix} \beta & 0 & 0 & 0 \\ 0 & 0 & 0 & 1 \end{bmatrix}, D = \begin{bmatrix} 1 \\ 0 \end{bmatrix}.$$

The system (11) with (10) for $t \in [t_k, t_{k+1})$ can be, further, written as

$$\dot{x}(t) = Ax(t) + BK[C_2 x(t_k - \theta_k) + Dv(t_k - \theta_k)] + F\Delta P_d(t). \tag{12}$$

Introducing the time-delay approach [11], the latter sampled-data control system (12) can be represented as

$$\dot{x}(t) = Ax(t) + BK[C_2 x(t - \vartheta(t) - \theta_k) + Dv(t - \vartheta(t) - \theta_k)] + F\Delta P_d(t), \tag{13}$$

where $\vartheta(t) = t - t_k$ for $t \in [t_k, t_{k+1})$. Now, our objective is to achieve frequency regulation (3) with reduced number of transmitted measurements in presence of time-delays and measurement disturbances.

III. Switching based event-trigger control

As in [33], we introduce a switching based continuous-time ET mechanism (see Fig. 2) to achieve our objectives. Let $h > 0$ be a waiting time. The sampling times s_k are constructed as follows. Let $\epsilon > 0$ be ET threshold and $\Omega \geq 0$ be a matrix. Given s_k, $k \in \mathbb{N}$, the ET mechanism waits for at least h seconds (thereby preventing infinite discrete transitions in a finite time, i.e, Zeno phenomenon) before the continuous-time ET condition:

$$(y(t) - y(s_k))^T \Omega (y(t) - y(s_k)) \geq \epsilon y^T(t) \Omega y(t), \tag{14}$$

is verified as continuous measurements are available. It means that ET mechanism starts working after h seconds

0885-8950 (c) 2020 IEEE. Personal use is permitted, but republication/redistribution requires IEEE permission. See http://www.ieee.org/publications_standards/publications/rights/index.html for more information.
Authorized licensed use limited to: TEL AVIV UNIVERSITY. Downloaded on June 06,2020 at 10:31:27 UTC from IEEE Xplore. Restrictions apply.

This article has been accepted for publication in a future issue of this journal, but has not been fully edited. Content may change prior to final publication. Citation information: DOI 10.1109/TPWRS.2020.2999488, IEEE Transactions on Power Systems

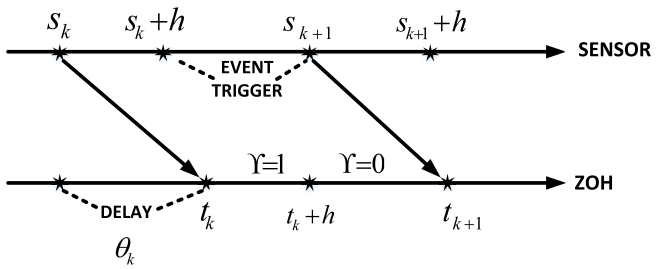

Fig. 2: Signal transmission under switching approach where the system is governed by periodic sampling during time instant $[t_k, t_k+h)$ and then by ET during $t \in [t_k+h, t_{k+1})$. Therefore two subsystems are created, each corresponding to $\Upsilon = 1$ and $\Upsilon = 0$

.

after the measurement is sent. As a result, the next measurement will be sent at least after h seconds if the ET condition violates. Thus, s_{k+1} is defined as [33]

$$s_{k+1} = \min\{t \geq s_k + h | \text{ ET condition in (14) holds}\}, \tag{15}$$

thereby transforming the controller (10) into an ETC controller $\bar{u}(t)$ as:

$$\bar{u}(t) = K\bar{y}(t) \tag{16}$$

where

$$\bar{y}(t) = \begin{cases} y(t), & \text{if (14) is true,} \\ y(s_k), & \text{if (14) is false.} \end{cases}$$

for $t \in [s_k + h, s_{k+1}]$. Denote by $e(t) = y(s_k) - y(t)$ for $t \in [s_k+h, s_{k+1}]$, the triggering error, we can further write (16) as

$$\bar{u}(t) = K[y(t) + e(t)].$$

Thus, in switching based ETC, the system (13), (15) is governed by the periodic sampling for $t \in [t_k, t_k+h)$, i.e., $t \in [s_k + \theta_k, s_k + \theta_k + h)$ and by continuous-time ET for $t \in [t_k + h, t_{k+1})$. Finally, in view of (15) and (16), the closed-loop system (13), can be presented as [33]

$$\begin{aligned} \dot{x}(t) =& Ax(t) + \Upsilon(t)BK[C_2x(t-\tau(t)) + Dv(t-\tau(t))] \\ &+(1-\Upsilon(t))BK[C_2x(t-\bar{\theta}(t)) + Dv(t-\bar{\theta}(t)) + e(t)] \\ &+F\Delta P_d(t), \end{aligned} \tag{17}$$

where

$$\begin{aligned} &\Upsilon(t) = \begin{cases} 1, & t \in [t_k, \min\{t_k+h, t_{k+1}\}), \\ 0, & t \in [\min\{t_k+h, t_{k+1}\}, t_{k+1}), \end{cases} \\ &\tau(t) = t - s_k, \ t \in [t_k, \min\{t_k+h, t_{k+1}\}), \\ &e(t) = y(s_k) - y(t-\bar{\theta}(t)), \ t \in [\min\{t_k+h, t_{k+1}\}, t_{k+1}), \end{aligned}$$

Note that $\tau(t)$ follows the relation: $\tau(t) \leq h + \theta_M := \tau_M$ and $\bar{\theta}(t) \in [0, \theta_M]$ is an unknown delay.

We are interested in determining the transmission times $\{s_k\}_{k\in\mathbb{N}}$ in order to guarantee the stability and performance. Precisely, our goal is, now, to internally exponentially stabilize (17) with (15), if it is exponentially stable with $\Delta P_d(t) \equiv 0$, $v(t) \equiv 0$. Furthermore, we redefine $\tau(t)$ as $\tau(t) = \bar{\theta}(t)$ for $t \in [t_k + h, t_{k+1})$ and let γ be the worst case L_2-gain under zero initial condition $x(0) = 0$ and $\Delta P_d, v$ such that $\Delta P_d^T(t)\Delta P_d(t) + v^T(t)v(t) \not\equiv 0$. Consider the following performance index [11]:

$$\begin{aligned} J = \int_0^\infty \{ & z^T(t)z(t) - \gamma^2 \left[\Delta P_d^T(t)\Delta P_d(t) \right. \\ & \left. + v^T(t-\tau(t))v(t-\tau(t))\right]\} dt, \end{aligned} \tag{18}$$

our objective is to establish $J < 0$ along the trajectories of (15),(17).

In pursuit of asymptotic stability and finite L_2-gain, we proposed the following theorem.

Theorem III.1. Consider the system (11) where $u(t) = \bar{u}(t)$. Given positive scalars γ, α, h, $\theta_M \geq 0$, $\epsilon \geq 0$, and $\tau_M = h + \theta_M$, let there exists $n \times n$ matrices $P > 0$, $\{S_i\}_{i=0,1} \geq 0$, $\{R_i\}_{i=0,1} \geq 0$, $\{G_i\}_{i=0,1} \geq 0$, and $m \times m$ matrix $\Omega \geq 0$ such that

$$\Gamma \leq 0, \ \Lambda \leq 0, \begin{bmatrix} R_0 & G_0 \\ G_0^T & R_0 \end{bmatrix} \geq 0, \ \begin{bmatrix} R_1 & G_1 \\ G_1^T & R_1 \end{bmatrix} \geq 0$$

where $\Gamma = \{\Gamma_{ij}\}$ and $\Lambda = \{\Lambda_{ij}\}$ are symmetric block matrices composed from the matrices

$$\begin{aligned} \Gamma_{11} =& \Lambda_{11} = A^TP + PA + 2\alpha P + S_0 - e^{-2\alpha\theta_M}R_0 + C_1^TC_1 \\ \Gamma_{12} =& e^{-2\alpha\theta_M}R_0 \\ \Gamma_{14} =& PBKC_2 \\ \Gamma_{15} =& \Lambda_{16} = PF \\ \Gamma_{16} =& \Lambda_{17} = PBKD \\ \Gamma_{17} =& \Lambda_{18} = A^T(\theta_M^2R_0 + h^2R_1) \\ \Gamma_{22} =& \Lambda_{22} = e^{-2\alpha\theta_M}(S_1 - S_0 - R_0) - e^{-2\alpha\tau_M}R_1 \\ \Gamma_{23} =& e^{-2\alpha\tau_M}G_1 \\ \Gamma_{24} =& e^{-2\alpha\tau_M}(R_1 - G_1) \\ \Gamma_{33} =& \Lambda_{33} = e^{-2\alpha\tau_M}(R_1 + S_1) \\ \Gamma_{34} =& e^{-2\alpha\tau_M}(R_1 - G_1^T) \\ \Gamma_{44} =& e^{-2\alpha\tau_M}(G_1 + G_1^T - 2R_1) \\ \Gamma_{47} =& \Lambda_{48} = (BKC_2)^T(\theta_M^2R_0 + h^2R_1) \\ \Gamma_{55} =& \Lambda_{66} = -\gamma^2I \\ \Gamma_{57} =& \Lambda_{68} = F^T(\theta_M^2R_0 + h^2R_1) \\ \Gamma_{77} =& \Lambda_{88} = -(\theta_M^2R_0 + h^2R_1) \\ \Gamma_{66} =& -\gamma^2I \\ \Gamma_{67} =& \Lambda_{78} = (BKD)^T(\theta_M^2R_0 + h^2R_1) \\ \Lambda_{12} =& e^{-2\alpha\theta_M}G_0 \\ \Lambda_{23} =& e^{-2\alpha\tau_M}R_1 \\ \Lambda_{24} =& e^{-2\alpha\theta_M}(R_0 - G_0^T) \\ \Lambda_{14} =& PBKC_2 + e^{-2\alpha\theta_M}(R_0 - G_0) \\ \Lambda_{15} =& PBK \\ \Lambda_{44} =& e^{-2\alpha\theta_M}(G_0 + G_0^T - 2R_0) + \epsilon C_2^T\Omega C_2 \\ \Lambda_{47} =& \epsilon C_2^T\Omega C_2 \\ \Lambda_{58} =& (BK)^T(\theta_M^2R_0 + h^2R_1) \\ \Lambda_{55} =& -\Omega \end{aligned}$$

0885-8950 (c) 2020 IEEE. Personal use is permitted, but republication/redistribution requires IEEE permission. See http://www.ieee.org/publications_standards/publications/rights/index.html for more information.
Authorized licensed use limited to: TEL AVIV UNIVERSITY. Downloaded on June 06,2020 at 10:31:27 UTC from IEEE Xplore. Restrictions apply.

This article has been accepted for publication in a future issue of this journal, but has not been fully edited. Content may change prior to final publication. Citation information: DOI 10.1109/TPWRS.2020.2999488, IEEE Transactions on Power Systems

$$\Lambda_{77} = \epsilon D^T \Omega D - \gamma^2 I,$$

rest blocks are null matrices. Then the controller (16) under the event-triggered sampling instants (15) internally exponentially stabilizes the system (11) with decay rate α and prescribed L_2-gain less than γ.

Proof is given in Appendix.

Remark III.2. The LMIs of Theorem III.1 are affine in A, B, F, therefore this approach is applicable to polytopic-type uncertainties.

Remark III.3. It is worth-noting that the Theorem III.1 signifies delay-dependent stability conditions. The delay-independent conditions are not applicable for LFC operation because when communication delay or fault exceeds some threshold, the LFC operation is ceased through voice communication or pause counter [10], [13].

IV. Switching approach for two-area power systems

We also deal with LFC operation of the two-area power systems. Assuming same generation units in all control areas ($i = 1, 2$), the dynamic model of each area is given by [14], [29]

$$\begin{aligned}
\Delta\dot{f}_i(t) &= -\frac{D_i}{M_i}\Delta f_i(t) + \frac{1}{M_i}\Delta P_{M,i}(t) - \frac{1}{M_i}\Delta P_{d,i}(t),\\
\Delta\dot{P}_{M,i}(t) &= -\frac{1}{T_{T,i}}\Delta P_{M,i}(t) + \frac{1}{T_{T,i}}\Delta P_{V,i}(t),\\
\Delta\dot{P}_{V,i}(t) &= -\frac{1}{T_{G,i}}\Delta P_{V,i}(t) - \frac{1}{R_i T_{G,i}}\Delta f_i(t) + \alpha_{G,i}\frac{1}{T_{G,i}}u_i(t).
\end{aligned} \tag{19}$$

The area control error $\Delta E(t)$ is

$$\Delta E_i(t) = \beta_i \Delta f_i(t) + \Delta P_{tie,i}(t)$$

where $\Delta P_{tie,i}(t)$ for $i = 1, 2$ is the net exchange of tie-line power of the ith control area given by

$$\Delta P_{tie,1}(t) = 2\pi T_{12}(\Delta f_1(t) - \Delta f_2(t))$$

and T_{12} is the tie-line synchronization coefficient between 1st and 2nd control area. Note that $\Delta P_{tie,1}(t) = -\Delta P_{tie,2}(t)$. Using (19), we can obtain complete model of the system similar to (11) where

$$x = \text{col}\left\{\Delta f_1, \Delta P_{M,1}, \Delta P_{V,1}, \int \Delta E_1, \Delta P_{tie}, \Delta f_2, \Delta P_{M,2}, \Delta P_{V,2}, \int \Delta E_2\right\} \in \mathbb{R}^9,\ \Delta P_d = \text{col}\{\Delta P_{d,1}, \Delta P_{d,2}\} \in \mathbb{R}^2,$$

$v = \text{col}\{v_1, v_2\} \in \mathbb{R}^2$,

$$A = \begin{bmatrix}
-\frac{D_1}{M_1} & \frac{1}{M_1} & 0 & 0 & -\frac{1}{M_1} & 0 & 0 & 0 & 0\\
0 & -\frac{1}{T_{T1}} & \frac{1}{T_{T1}} & 0 & 0 & 0 & 0 & 0 & 0\\
-\frac{1}{R_1 T_{G1}} & 0 & -\frac{1}{T_{G1}} & 0 & 0 & 0 & 0 & 0 & 0\\
\beta & 0 & 0 & 0 & 1 & 0 & 0 & 0 & 0\\
2\pi T_{12} & 0 & 0 & 0 & 0 & -2\pi T_{12} & 0 & 0 & 0\\
0 & 0 & 0 & 0 & \frac{1}{M_2} & -\frac{D_2}{M_2} & \frac{1}{M_2} & 0 & 0\\
0 & 0 & 0 & 0 & 0 & 0 & -\frac{1}{T_{T2}} & \frac{1}{T_{T2}} & 0\\
0 & 0 & 0 & 0 & 0 & -\frac{1}{R_2 T_{G2}} & 0 & -\frac{1}{T_{G2}} & 0\\
0 & 0 & 0 & 0 & -1 & \beta & 0 & 0 & 0
\end{bmatrix},$$

$$B = \begin{bmatrix} 0 & 0 & \frac{1}{T_{G1}} & 0 & 0 & 0 & 0 & 0 & 0\\ 0 & 0 & 0 & 0 & 0 & 0 & 0 & \frac{1}{T_{G2}} & 0 \end{bmatrix}^\top,$$

$$F = \begin{bmatrix} -\frac{1}{M_1} & 0 & 0 & 0 & 0 & 0 & 0 & 0 & 0\\ 0 & 0 & 0 & 0 & 0 & -\frac{1}{M_2} & 0 & 0 & 0 \end{bmatrix}^\top,$$

$$C_1 = \begin{bmatrix} 1 & 0 & 0 & 0 & 0 & 0 & 0 & 0 & 0\\ 0 & 0 & 0 & 0 & 0 & 1 & 0 & 0 & 0 \end{bmatrix},$$

$$C_2 = \begin{bmatrix} \beta & 0 & 0 & 0 & 1 & 0 & 0 & 0 & 0\\ 0 & 0 & 0 & 1 & 0 & 0 & 0 & 0 & 0\\ 0 & 0 & 0 & 0 & -1 & \beta & 0 & 0 & 0\\ 0 & 0 & 0 & 0 & 0 & 0 & 0 & 0 & 1 \end{bmatrix},\ D = \begin{bmatrix} 1 & 0\\ 0 & 0\\ 0 & 1\\ 0 & 0 \end{bmatrix}^\top,$$

and the controller $u(t) = Ky(t)$ where

$$K = \begin{bmatrix} k_{P1} & k_{I1} & 0 & 0\\ 0 & 0 & k_{P2} & k_{I2} \end{bmatrix}.$$

Following the same methodology as described in section III, we can obtain the same results as mentioned in Theorem III.1 to impose switching based ETC.

V. Switching approach for power system with EV

We also study the power system network in which the electric vehicles are integrated to participate in LFC. As in [18], [34], the aggregated EVs are considered without battery state of charge and the dynamics of generation unit (in addition to (1)) is expressed as

$$\Delta\dot{P}_E(t) = -\frac{1}{T_E}\Delta P_E(t) - \frac{K_E}{RT_E}\Delta f(t) + \alpha_E \frac{K_E}{T_E}u(t) \tag{20}$$

where K_E, T_E, α_E are gain, time-constant and participation factor, respectively. The dynamical model has the form (11) where $x = \text{col}\{\Delta f, \Delta P_M, \Delta P_V, \Delta P_E, \Delta E\} \in \mathbb{R}^5$,

$$A = \begin{bmatrix}
-\frac{D}{M} & \frac{1}{M} & 0 & \frac{1}{M} & 0\\
0 & -\frac{1}{T_T} & \frac{1}{T_T} & 0 & 0\\
-\frac{1}{RT_G} & 0 & -\frac{1}{T_G} & 0 & 0\\
-\frac{K_E}{RT_E} & 0 & 0 & -\frac{1}{T_E} & 0\\
\beta & 0 & 0 & 0 & 0
\end{bmatrix},\ B = \begin{bmatrix} 0\\ 0\\ \frac{\alpha_G}{T_G}\\ \frac{\alpha_E}{T_E}\\ 0 \end{bmatrix},$$

$$F = \begin{bmatrix} -\frac{1}{M} & 0 & 0 & 0 & 0 \end{bmatrix}^\top,\ C_1 = [1\ 0\ 0\ 0\ 0],$$

$$C_2 = \begin{bmatrix} \beta & 0 & 0 & 0 & 0\\ 0 & 0 & 0 & 0 & 1 \end{bmatrix},\ D = \begin{bmatrix} 1\\ 0 \end{bmatrix}.$$

Applying the approach as mentioned in the section III, we can obtain the similar results as stated in Theorem III.1.

0885-8950 (c) 2020 IEEE. Personal use is permitted, but republication/redistribution requires IEEE permission. See http://www.ieee.org/publications_standards/publications/rights/index.html for more information.
Authorized licensed use limited to: TEL AVIV UNIVERSITY. Downloaded on June 06,2020 at 10:31:27 UTC from IEEE Xplore. Restrictions apply.

This article has been accepted for publication in a future issue of this journal, but has not been fully edited. Content may change prior to final publication. Citation information: DOI 10.1109/TPWRS.2020.2999488, IEEE Transactions on Power Systems

TABLE I: Maximum h and average SM for case 1

	Periodic	Event-trigger	Switching approach
h	0.5	0.56	0.64
SM	117	41	36

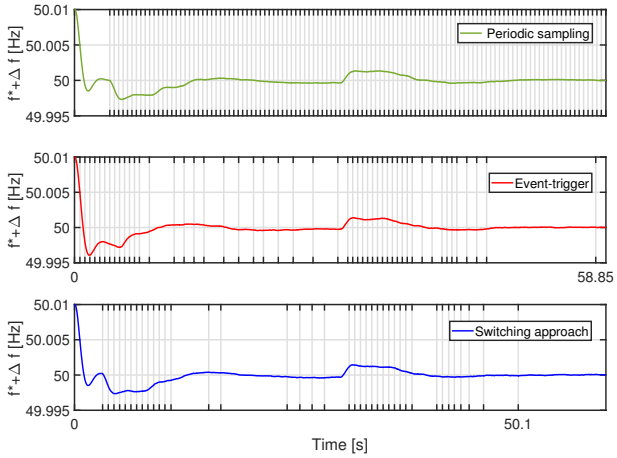

Fig. 3: Time evolution of frequency deviation for case 1

TABLE II: Maximum h and average SM for case 2

	Periodic	Event-trigger	Switching approach
h	2.3	0.7	1
SM	35	14	12

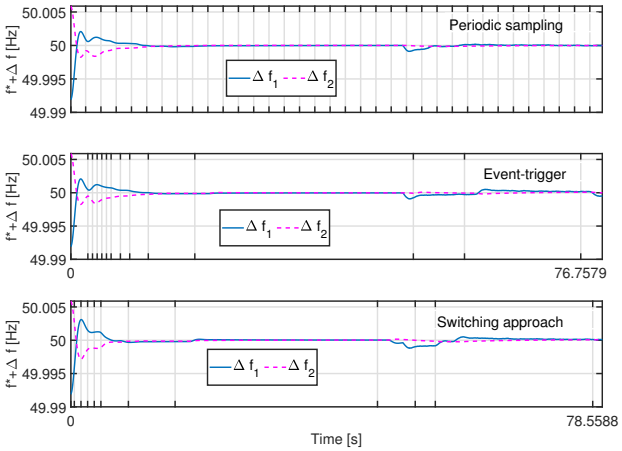

Fig. 4: Time evolution of frequency deviation under periodic sampling, event-trigger and switching approach

VI. Simulation Studies

To illustrate the effectiveness of proposed approach, three case studies have been carried out. With the given stabilizing controller, we compared three approaches of selecting sampling instants:

1) Periodic sampling with $s_k = ih$, $i \in \mathbb{N}$ where maximum h can be calculated by setting $\epsilon = 0$ in (14) and employing [33, Proposition 1].
2) Periodic event-triggering [22]

$$s_{k+1} = \min\{s_k + ih | i \in \mathbb{N},\ \Xi > 0\} \tag{21}$$

where $\Xi = ((y(s_k + ih) - y(s_k))^T \Omega (y(s_k + ih) - y(s_k))) - \epsilon y^T(s_k + ih)\Omega y(s_k + ih)$ is ET condition; maximum h can be obtained by setting $\Upsilon(t) = 0$ and $\bar{\theta}(t) \leq \theta_M$ in (17) and modifying the proof of [28, Theorem 2].
3) The proposed switching approach with sampling rule defined in (15) where maximum h satisfies Theorem III.1.

Remark VI.1. The switching approach outperforms the periodic event-triggering in the sense that the sensor has to wait for at least $2h$ time after the measurement is sent when the ET mechanism follows (21) whereas it waits for atleast h time in switching approach.

All the calculations and simulations are conducted using MATLAB 9.5 (R2018b). Computations for LMI are carried out in the MATLAB-based software package YALMIP [35] and are solved using SDPT3-4.0 [36].

A. Case 1: Single-area system

We consider a single-area power network whose dynamic model is described in section II and is governed by the (11). The standard nominal values of the parameters are

$$D = 1, M = 10, T_T = 0.3, T_G = 0.1, R = 0.05 \tag{22}$$

and $\beta = 1 + 1/R$ [19], [29]. The stabilizing PI parameters chosen are $k_P = -0.1$ and $k_I = -0.2$. For the analysis, the network-induced delay $\theta_M = 4$ s is considered. For $\epsilon = 0.003, \alpha = 0.01, \gamma = 1$, we obtained the maximum h as given in Table I which depicts that the sampling time is more for the proposed approach. We simulate the system for load disturbance (in p.u.)

$$\Delta P_d(t) = \begin{cases} 0.005\sin(0.4t), & 0 < t < 10 \\ 0.01, & \text{otherwise} \end{cases} \tag{23}$$

and networked-induced disturbance (in p.u.)

$$v(t) = \begin{cases} 0.1, & 0 < t < 10 \\ 0.01t, & 10 < t < 30 \\ 0.01(1 + r), & \text{otherwise} \end{cases} \tag{24}$$

where r is a single uniformly distributed random number in the interval (0,1). It is observed from Fig. 3 that the deviation in frequency from $f^* = 50$ Hz converges to zero (i.e., f^*) for initial condition $x_0 = [0.01, 0, 0, 0]$. We further performed numerical simulations for several initial conditions given by $x(0) = 0.01[\cos(l\pi/5), \sin(l\pi/5), \cos(l\pi/5), \sin(l\pi/5)]$ with $l = 1, \ldots, 4$ and it is also evident from Table I that the average sent measurements (SM) are approximately 12% less than periodic event-triggered sampling. Thus the network load is reduced while handling the induced delays and disturbances both emanating due to load and network.

0885-8950 (c) 2020 IEEE. Personal use is permitted, but republication/redistribution requires IEEE permission. See http://www.ieee.org/publications_standards/publications/rights/index.html for more information.
Authorized licensed use limited to: TEL AVIV UNIVERSITY. Downloaded on June 06,2020 at 10:31:27 UTC from IEEE Xplore. Restrictions apply.

This article has been accepted for publication in a future issue of this journal, but has not been fully edited. Content may change prior to final publication. Citation information: DOI 10.1109/TPWRS.2020.2999488, IEEE Transactions on Power Systems

B. Case 2: Two-area system

We extend our study to two-area system with identical parameter (22) and stabilizing controller. For the analysis, the network-induced delay $\theta_M = 3$ s is considered. For $\epsilon = 0.001, \alpha = 0.01, \gamma = 100$, we obtained the maximum h as given in Table II which depicts that the sampling time is more for the proposed approach. We simulate the system for $v(t) = 0.01(1 + r)$. Let the load disturbance $\Delta P_{d,1}(t) = 0.01$ for all $t > 50$ s occurs in area 1 whereas in area 2, it is $\Delta P_{d,2}(t) = 0.01$ p.u. for all $t > 0$. The simulation results shown in Fig. 4 confirm that the deviation in frequencies in both areas converge to zero (f^*) for the initial condition $x_0 = [0.0075, 0, 0, 0, 0, 0.005, 0, 0, 0]$. The behavior is further confirmed for several initial conditions given by

$$x(0) = 0.01\,(\cos(l\pi/5), \sin(l\pi/5), \cos(l\pi/5), \sin(l\pi/5), \cos(l\pi/5), \sin(l\pi/5), \cos(l\pi/5), \sin(l\pi/5), \cos(l\pi/5))$$

with $l = 1, \ldots, 9$ and found that the average sent measurements are approximately 15% less than periodic event-triggered sampling.

We also treat the system under measurement disturbance as cyber-attack where the following typical time-varying attack signal[1] from [4] is applied:

$$v(t) = \begin{cases} 0.2, & 0 < t < 5 \\ 0.5\sin(2t) + \frac{0.5}{t^2}, & 5 < t < 20 \\ 0.2\sin(t), & 20 < t < 30 \\ 0.3\cos(t), & \text{otherwise.} \end{cases}$$

The system is simulated for total 80 s and under load fluctuation of 0.1 p.u. The response for initial condition $x(0) = 10^{-3} \times (3.1,\ 3.1,\ 9.5,\ 3.1,\ 9.5,\ 3.1,\ 9.5,\ 3.1)$ is shown in Fig. 5 which states that the frequency deviations are bounded in the acceptable range. The amount of sent messages are 35, 25 and 22 under periodic sampling, event-trigger and switching approach, respectively.

C. Case 3: Single-area system with electric vehicle

Lastly to validate the switching approach in deregulated scenario, we study a single-area power system where EV ($K_E = 1 = T_E$) takes part in LFC operation. For the analysis under network-induced delay $\theta_M = 1.2$ s, $\epsilon = 0.001, \alpha = 0.01, \gamma = 20, k_P = -0.1, k_I = -0.5$, we obtained the maximum h as given in Table III which depicts that the sampling time is more for the proposed approach. We simulate the system for $\Delta P_d(t) = 0.01(1 + r) = v(t)$ and the results in Fig. 6 exhibit that the deviation in frequency converges to zero for zero (i.e., $f^* = 50$ Hz) initial condition. We carried out simulations for several initial conditions given by $x(0) = 0.01\,[\cos(l\pi/5), \sin(l\pi/5), \cos(l\pi/5), \sin(l\pi/5), \cos(l\pi/5)]$ with $l = 1, ..., 5$ and observe that the average sent measurements are approximately 20% less than periodic event-trigger sampling.

[1]Attack signal are considered according to the National Electric Sector Cybersecurity Organization Resource (NESCOR) standard. See [4] and references therein.

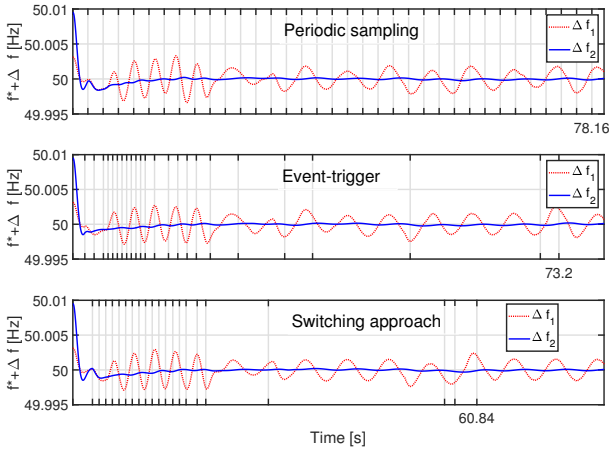

Fig. 5: Time evolution of frequency deviation under cyber attack scenario

TABLE III: Maximum h and average SM for case 3

	Periodic	Event-trigger	Switching approach
h	0.82	0.72	0.765
SM	62	15	12

D. Case 4: Two-area system with different generation units

The switching approach can be extended to the multi-area power systems having different generation unit in all control areas. For this, the case study has been extended to two-area power system where control area 1 has thermal power plant while the control area 2 consists of hydro-power plant[2]. The model of the complete system acquires

[2]Due to the space limitation, the complete description is omitted. The reader can refer to [37] for more details.

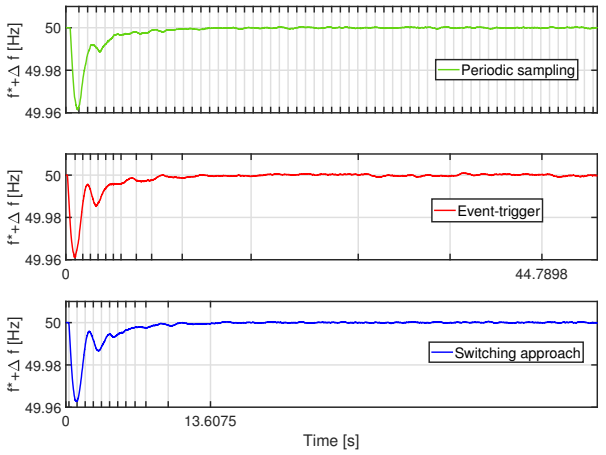

Fig. 6: Time evolution of frequency deviation for case 3

0885-8950 (c) 2020 IEEE. Personal use is permitted, but republication/redistribution requires IEEE permission. See http://www.ieee.org/publications_standards/publications/rights/index.html for more information.
Authorized licensed use limited to: TEL AVIV UNIVERSITY. Downloaded on June 06,2020 at 10:31:27 UTC from IEEE Xplore. Restrictions apply.

This article has been accepted for publication in a future issue of this journal, but has not been fully edited. Content may change prior to final publication. Citation information: DOI 10.1109/TPWRS.2020.2999488, IEEE Transactions on Power Systems

TABLE IV: Average measurement sent for case 4

	Periodic	Event-trigger	Switching approach
h	0.015	0.012	0.018
SM	2000	564	500

the form (11) where

$$x = \text{col}\left\{\Delta f_1, \Delta P_{g,1}, \Delta X_{g,1}, \int \Delta E_1, \Delta P_{tie}, \Delta f_2, \Delta P_{g,2}, \Delta X_{g,2}, \Delta X_{gh,2}, \int \Delta E_2\right\} \in \mathbb{R}^{10},$$

$\Delta P_d = \text{col}\{\Delta P_{d,1}, \Delta P_{d,2}\} \in \mathbb{R}^2$, $v = \text{col}\{v_1, v_2\} \in \mathbb{R}^2$. The system matrices are as follows:

$$A = \begin{bmatrix} -\frac{1}{T_{P1}} & \frac{K_{P1}}{T_{P1}} & 0 & 0 & -\frac{K_{P1}}{T_{P1}} & 0 & 0 & 0 & 0 & 0 \\ 0 & -\frac{1}{T_{T1}} & \frac{1}{T_{T1}} & 0 & 0 & 0 & 0 & 0 & 0 & 0 \\ -\frac{1}{R_1 T_{G1}} & 0 & -\frac{1}{T_{G1}} & 0 & 0 & 0 & 0 & 0 & 0 & 0 \\ \beta_1 & 0 & 0 & 0 & 1 & 0 & 0 & 0 & 0 & 0 \\ 2\pi T_{12} & 0 & 0 & 0 & 0 & -2\pi T_{12} & 0 & 0 & 0 & 0 \\ 0 & 0 & 0 & 0 & \frac{K_{P2}}{T_{P2}} & -\frac{1}{T_{P2}} & \frac{K_{P2}}{T_P} & 0 & 0 & 0 \\ 0 & 0 & 0 & 0 & 0 & 2J_1 & -\frac{2}{T_w} & 2J_3 & 2J_2 & 0 \\ 0 & 0 & 0 & 0 & 0 & -J_1 & 0 & \frac{-1}{T_2} & -J_2 & 0 \\ 0 & 0 & 0 & 0 & 0 & -\frac{1}{R_2 T_{G2}} & 0 & 0 & \frac{-1}{T_1} & 0 \\ 0 & 0 & 0 & 0 & -1 & \beta_2 & 0 & 0 & 0 & 0 \end{bmatrix},$$

$$B = \begin{bmatrix} 0 & 0 & \frac{1}{T_{G1}} & 0 & 0 & 0 & 0 & 0 & 0 & 0 \\ 0 & 0 & 0 & 0 & 0 & 0 & 0 & 0 & \frac{1}{T_1} & 0 \end{bmatrix}^\top,$$

$$F = \begin{bmatrix} \frac{-K_{P1}}{T_{P1}} & 0 & 0 & 0 & 0 & 0 & 0 & 0 & 0 & 0 \\ 0 & 0 & 0 & 0 & 0 & \frac{-K_{P2}}{T_{P2}} & 0 & 0 & 0 & 0 \end{bmatrix}^\top,$$

$$C_1 = \begin{bmatrix} 1 & 0 & 0 & 0 & 0 & 0 & 0 & 0 & 0 & 0 \\ 0 & 0 & 0 & 0 & 0 & 1 & 0 & 0 & 0 & 0 \end{bmatrix},$$

$$C_2 = \begin{bmatrix} \beta_1 & 0 & 0 & 0 & 1 & 0 & 0 & 0 & 0 & 0 \\ 0 & 0 & 0 & 1 & 0 & 0 & 0 & 0 & 0 & 0 \\ 0 & 0 & 0 & 0 & -1 & \beta_2 & 0 & 0 & 0 & 0 \\ 0 & 0 & 0 & 0 & 0 & 0 & 0 & 0 & 0 & 1 \end{bmatrix}, \quad D = \begin{bmatrix} 1 & 0 \\ 0 & 0 \\ 0 & 1 \\ 0 & 0 \end{bmatrix}^\top,$$

$$J_1 = \frac{T_r}{T_1 T_2 R_2}, \quad J2 = \frac{T_r - T_1}{T_1 T_2}, \quad J3 = \frac{T_2 + T_w}{T_w T_2}.$$

The nominal values for simulation are taken as: $T_{G1} = 0.08$, $T_{T1} = 0.3$, $K_{P1} = 120$, $T_{P1} = 20$, $R_1 = 2.4 = R_2$, $\beta_1 = 0.425$, $T_{12} = 0.086$, $K_{P2} = 80$, $T_{P2} = 20$, $T_1 = 48.7$, $T_2 = 5$, $R_2 = 2.4$, $T_w = 1, T_r = 0.6, \beta_2 = 0.5$. The analysis has been considered for $\theta_M = 0.02$ s, $\epsilon = 0.001, \alpha = 0.01, \gamma = 100, k_{P1} = 1.9, k_{I1} = 0.5, k_{P2} = 1.15, k_{I2} = 0.1$. Fig. 7 represents the state response $(\Delta f_1, \Delta f_2)$ for $\Delta P_{d1} = 0.01$ and initial conditions $x_0 = 0.1[0.95, 0.31, 0.95, 0.31, 0.95, 0.31, 0.95, 0.31, 0.95, 0.31]$; and Table IV represent the superiority of the switching approach due to reduced number of sent messages.

E. Case 5: Multi-area system with multi generation units

To examine the efficiency of the proposed approach, we consider another two-area power system where each control area consists of two thermal generation units. Refer

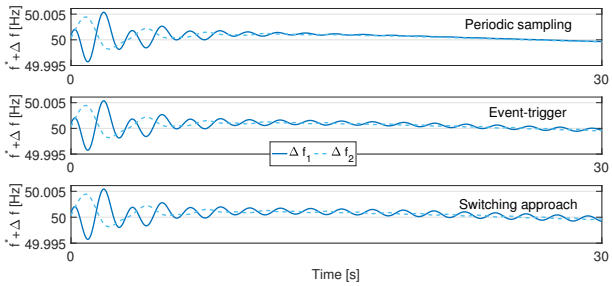

Fig. 7: Time evolution of frequency deviation for case 4

[38] for details. The system follows the standard model (11) where

$$x = \text{col}\left\{\Delta P_{V,11}, \Delta P_{V,12}, \Delta P_{M,11}, \Delta P_{M,12}, \Delta f_1, \int \Delta E_1, \Delta P_{tie}, \Delta P_{V,21}, \Delta P_{V,22}, \Delta P_{M,21}, \Delta P_{M,22}, \Delta f_2, \int \Delta E_2\right\} \in \mathbb{R}^{13},$$

$\Delta P_d = \text{col}\{\Delta P_{d,1}, \Delta P_{d,2}\} \in \mathbb{R}^2$, $v = \text{col}\{v_1, v_2\} \in \mathbb{R}^2$. The system matrices are:

$$A = \begin{bmatrix} \frac{-1}{T_{G11}} & 0 & 0 & 0 & \frac{-1}{T_{G11}R_1} & 0 & 0 & 0 & 0 & 0 & 0 & 0 & 0 \\ 0 & \frac{-1}{T_{G12}} & 0 & 0 & \frac{-1}{T_{G12}R_{12}} & 0 & 0 & 0 & 0 & 0 & 0 & 0 & 0 \\ \frac{1}{T_{T11}} & 0 & \frac{-1}{T_{T12}} & 0 & 0 & 0 & 0 & 0 & 0 & 0 & 0 & 0 & 0 \\ 0 & \frac{1}{T_{T12}} & 0 & \frac{-1}{T_{T12}} & 0 & 0 & 0 & 0 & 0 & 0 & 0 & 0 & 0 \\ 0 & 0 & \frac{1}{M_1} & \frac{1}{M_1} & \frac{-D_1}{M_1} & 0 & \frac{-1}{M_1} & 0 & 0 & 0 & 0 & 0 & 0 \\ 0 & 0 & 0 & 0 & \beta & 0 & 1 & 0 & 0 & 0 & 0 & 0 & 0 \\ 0 & 0 & 0 & 0 & T_{12} & 0 & 0 & 0 & 0 & 0 & 0 & -T_{12} & 0 \\ 0 & 0 & 0 & 0 & 0 & 0 & 0 & \frac{-1}{T_{G21}} & 0 & 0 & 0 & \frac{-1}{T_{G21}R_{21}} & 0 \\ 0 & 0 & 0 & 0 & 0 & 0 & 0 & 0 & \frac{-1}{T_{G22}} & 0 & 0 & \frac{-1}{T_{G22}R_{22}} & 0 \\ 0 & 0 & 0 & 0 & 0 & 0 & 0 & \frac{1}{T_{T21}} & 0 & \frac{-1}{T_{T21}} & 0 & 0 & 0 \\ 0 & 0 & 0 & 0 & 0 & 0 & 0 & 0 & \frac{1}{T_{T22}} & 0 & \frac{-1}{T_{T22}} & 0 & 0 \\ 0 & 0 & 0 & 0 & 0 & 0 & \frac{1}{M_2} & 0 & 0 & \frac{1}{M_2} & \frac{1}{M_2} & \frac{-D_2}{M_2} & 0 \\ 0 & 0 & 0 & 0 & 0 & 0 & -1 & \beta & 0 & 0 & 0 & 0 & 0 \end{bmatrix},$$

$$B = \begin{bmatrix} \frac{\alpha_1}{T_{G11}} & \frac{\alpha_1}{T_{G12}} & 0 & 0 & 0 & 0 & 0 & 0 & 0 & 0 & 0 & 0 & 0 \\ 0 & 0 & 0 & 0 & 0 & 0 & 0 & \frac{\alpha_2}{T_{G21}} & \frac{\alpha_2}{T_{G22}} & 0 & 0 & 0 & 0 \end{bmatrix}^\top,$$

$$F = \begin{bmatrix} 0 & 0 & 0 & 0 & \frac{1}{M_1} & 0 & 0 & 0 & 0 & 0 & 0 & 0 & 0 \\ 0 & 0 & 0 & 0 & 0 & 0 & 0 & 0 & 0 & 0 & 0 & \frac{1}{M_2} & 0 \end{bmatrix}^\top,$$

$$C_1 = \begin{bmatrix} 0 & 0 & 0 & 0 & 1 & 0 & 0 & 0 & 0 & 0 & 0 & 0 & 0 \\ 0 & 0 & 0 & 0 & 0 & 0 & 0 & 0 & 0 & 0 & 0 & 1 & 0 \end{bmatrix},$$

$$C_2 = \begin{bmatrix} 0 & 0 & 0 & 0 & \beta & 0 & 1 & 0 & 0 & 0 & 0 & 0 & 0 \\ 0 & 0 & 0 & 0 & 0 & 1 & 0 & 0 & 0 & 0 & 0 & 0 & 0 \\ 0 & 0 & 0 & 0 & 0 & 0 & -1 & 0 & 0 & 0 & 0 & \beta & 0 \\ 0 & 0 & 0 & 0 & 0 & 0 & 0 & 0 & 0 & 0 & 0 & 0 & 1 \end{bmatrix}, \quad D = \begin{bmatrix} 1 & 0 \\ 0 & 0 \\ 0 & 1 \\ 0 & 0 \end{bmatrix}^\top,$$

For simulations, the standard nominal parameters selected are: $T_{G11} = 0.06 = T_{G21}, T_{G12} = 0.07 = T_{G22}, R_{11} = 2.4 = R_{21}, R_{12} = 3.3 = R_{22}, T_{T11} = 0.36 = T_{T21}, T_{T12} = 0.42 = T_{T21}, M_1 = 0.1667 = M_2, D_1 = 0.0084 = D_2, \beta_1 = 0.8675 = \beta_2, \alpha_1 = \alpha_2 = 0.5, T_{12} = 0.1986$.The analysis is conducted for $\theta_M = 0.8$ s, $\epsilon = 0.001, \alpha = 0.01, \gamma = 100, k_{P1} = -0.1 = k_{P2}, k_{I1} = 0.45 = k_{I2}$. It can be observed in Fig. 8 that the frequencies in both the areas reaches to the schedule $f^* = 50$ Hz for $\Delta P_{d1} = 0.01$ and initial conditions

$$x_0 = 0.01\,[0.81, 0.59, 0.81, 0.59, 0.81, 0.59, 0.81, 0.59, 0.81, 0.59, 0.81, 0.59, 0.81]\,.$$

Lastly, Table V exhibits that least messages are sent to stabilize the frequency.

0885-8950 (c) 2020 IEEE. Personal use is permitted, but republication/redistribution requires IEEE permission. See http://www.ieee.org/publications_standards/publications/rights/index.html for more information.
Authorized licensed use limited to: TEL AVIV UNIVERSITY. Downloaded on June 06,2020 at 10:31:27 UTC from IEEE Xplore. Restrictions apply.

This article has been accepted for publication in a future issue of this journal, but has not been fully edited. Content may change prior to final publication. Citation information: DOI 10.1109/TPWRS.2020.2999488, IEEE Transactions on Power Systems

TABLE V: Average measurement sent for case 5

	Periodic	Event-trigger	Switching approach
h	0.15	0.07	0.08
SM	130	214	203

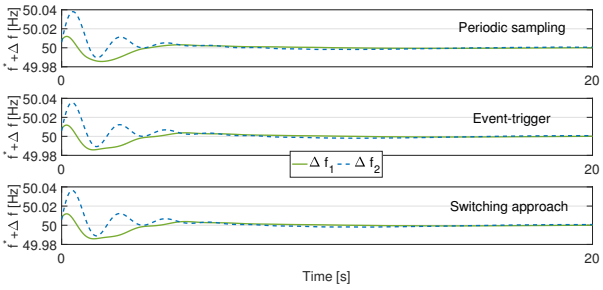

Fig. 8: Time evolution of frequency deviation for case 5

Remark VI.2. Both EV and distributed generation (e.g., renewable energy sources, battery energy storage system) are trending these days for study of LFC operation. The switching approach is equally applicable to these generation units under networked induced time-varying delays and disturbances.

Remark VI.3. The proposed switching approach can be implemented on a large-scale analog power system simulator to illustrate its capability in real-time LFC applications. The control scheme including PI controller and ET mechanism can be built in a personal computer (PC), and connected to the power system hardware by means of a digital signal processing board equipped with analog-to-digital and digital-to-analog converters. The bounded but time-varying delays and disturbance in the measurement and control signals can be artificially induced through PC.

Remark VI.4. Note that the maximum h of the periodic sampling, in all the cases, can vary from smallest to largest in comparison to that of the switching approach. There is no any possible reason for it. One can only obtain the maximum h that ensures stability by means of [33, Proposition 1] with $\epsilon = 0$.

VII. Conclusions

We have considered the LFC problem with respect to time-varying networked-induced delay and measurement disturbance. For this set-up, we have introduced a new switching based event-triggered control approach and derived the sufficient delay dependent stability conditions to ensure the lower bound for inter-events during validation of event-trigger conditions. This helps in reducing the workload of power network while maintaining stability and performance. The approach has been applied to different power systems configuration comprising single- and multi-area, and single-area with integrated EV.

One limitation of this work is that the measurements ($\Delta f_i(t)$ signals) are checked by the centrally located ET machine in case of multi-area system. This leads to increased computational complexity and poor scalability of central control scheme. A decentralized control approach is one of the promising solution which is our future work. Besides, we will also seek the solution for false intrusion mitigation and overall failure detection in the LFC operation of power systems. Delay bounds will help in providing guidelines to mitigate such attacks and faults.

Acknowledgment

The authors are thankful to Dr. Anton Selivanov (The University of Sheffield) for his help in simulations and Rami Katz (Tel Aviv University) for useful discussions.

References

[1] H. Bevrani and T. Hiyama, Intelligent automatic generation control. CRC press, 2016.

[2] A. Pappachen and A. P. Fathima, "Critical research areas on load frequency control issues in a deregulated power system: A state-of-the-art-of-review," Renewable and Sustainable Energy Reviews, vol. 72, pp. 163–177, 2017.

[3] M. Gheisarnejad, M.-H. Khooban, and T. Dragicevic, "The future 5G network based secondary load frequency control in maritime microgrids," IEEE Journal of Emerging and Selected Topics in Power Electronics, 2019.

[4] H. H. Alhelou, M. E. H. Golshan, and N. D. Hatziargyriou, "A decentralized functional observer based optimal LFC considering unknown inputs, uncertainties and cyber-attacks," IEEE Transactions on Power Systems, 2019.

[5] S. Saxena, "Load frequency control strategy via fractional-order controller and reduced-order modeling," International Journal of Electrical Power & Energy Systems, vol. 104, pp. 603–614, 2019.

[6] S. Saxena and Y. V. Hote, "Decentralized PID load frequency control for perturbed multi-area power systems," International Journal of Electrical Power & Energy Systems, vol. 81, pp. 405–415, 2016.

[7] ——, "Stabilization of perturbed system via IMC: An application to load frequency control," Control Engineering Practice, vol. 64, pp. 61–73, 2017.

[8] S. Hanwate, Y. V. Hote, and S. Saxena, "Adaptive policy for load frequency control," IEEE Transactions on Power Systems, vol. 33, no. 1, pp. 1142–1144, 2018.

[9] S. Bhowmik, K. Tomsovic, and A. Bose, "Communication models for third party load frequency control," IEEE Transactions on Power Systems, vol. 19, no. 1, pp. 543–548, 2004.

[10] X. Yu and K. Tomsovic, "Application of linear matrix inequalities for load frequency control with communication delays," IEEE transactions on power systems, vol. 19, no. 3, pp. 1508–1515, 2004.

[11] E. Fridman, Introduction to time-delay systems: Analysis and control. Springer, 2014.

[12] J. Schiffer, F. Dörfler, and E. Fridman, "Robustness of distributed averaging control in power systems: Time delays & dynamic communication topology," Automatica, vol. 80, pp. 261–271, 2017.

[13] C.-K. Zhang, L. Jiang, Q. Wu, Y. He, and M. Wu, "Delay-dependent robust load frequency control for time delay power systems," IEEE Transactions on Power Systems, vol. 28, no. 3, pp. 2192–2201, 2013.

[14] K. Ramakrishnan and G. Ray, "Stability criteria for nonlinearly perturbed load frequency systems with time-delay," IEEE Journal on Emerging and Selected Topics in Circuits and Systems, vol. 5, no. 3, pp. 383–392, 2015.

[15] F. Yang, J. He, and D. Wang, "New stability criteria of delayed load frequency control systems via infinite-series-based inequality," IEEE Transactions on Industrial Informatics, vol. 14, no. 1, pp. 231–240, 2017.

[16] F. Yang, J. He, and Q. Pan, "Further improvement on delay-dependent load frequency control of power systems via truncated B–L inequality," IEEE Transactions on Power Systems, vol. 33, no. 5, pp. 5062–5071, 2018.

[17] P. Ojaghi and M. Rahmani, "LMI-based robust predictive load frequency control for power systems with communication delays," IEEE Transactions on Power Systems, vol. 32, no. 5, pp. 4091–4100, 2017.

[18] T. N. Pham, S. Nahavandi, H. Trinh, K. P. Wong et al., "Static output feedback frequency stabilization of time-delay power systems with coordinated electric vehicles state of charge control," IEEE Transactions on Power Systems, vol. 32, no. 5, pp. 3862–3874, 2017.

[19] C. Ramlal, A. Singh, S. Rocke, and M. Sutherland, "Decentralized fuzzy H_∞ iterative learning lfc with time-varying communication delays and parametric uncertainties," IEEE Transactions on Power Systems, pp. 1–1, 2019.

[20] J. M. Thangaiah and R. Parthasarathy, "Delay-dependent stability analysis of power system considering communication delays," International Transactions on Electrical Energy Systems, vol. 27, no. 3, p. e2260, 2017.

[21] L. Jin, C.-K. Zhang, Y. He, L. Jiang, and M. Wu, "Delay-dependent stability analysis of multi-area load frequency control with enhanced accuracy and computation efficiency," IEEE Transactions on Power Systems, 2019.

0885-8950 (c) 2020 IEEE. Personal use is permitted, but republication/redistribution requires IEEE permission. See http://www.ieee.org/publications_standards/publications/rights/index.html for more information.
Authorized licensed use limited to: TEL AVIV UNIVERSITY. Downloaded on June 06,2020 at 10:31:27 UTC from IEEE Xplore. Restrictions apply.

This article has been accepted for publication in a future issue of this journal, but has not been fully edited. Content may change prior to final publication. Citation information: DOI 10.1109/TPWRS.2020.2999488, IEEE Transactions on Power Systems

[22] K. Liu, A. Selivanov, and E. Fridman, "Survey on time-delay approach to networked control," Annual Reviews in Control, 2019.

[23] S. Wen, X. Yu, Z. Zeng, and J. Wang, "Event-triggering load frequency control for multiarea power systems with communication delays," IEEE Transactions on Industrial Electronics, vol. 63, no. 2, pp. 1308–1317, 2016.

[24] X. Su, X. Liu, and Y.-D. Song, "Event-triggered sliding-mode control for multi-area power systems," IEEE Transactions on Industrial Electronics, vol. 64, no. 8, pp. 6732–6741, 2017.

[25] L. Dong, Y. Tang, H. He, and C. Sun, "An event-triggered approach for load frequency control with supplementary ADP," IEEE Transactions on Power Systems, vol. 32, no. 1, pp. 581–589, 2016.

[26] Z. Wu, H. Mo, J. Xiong, and M. Xie, "Adaptive event-triggered observer-based output feedback $\mathcal{L}_\infty$ load frequency control for networked power systems," IEEE Transactions on Industrial Informatics, 2019.

[27] C. Peng, J. Zhang, and H. Yan, "Adaptive event-triggering H_∞ load frequency control for network-based power systems," IEEE Transactions on Industrial Electronics, vol. 65, no. 2, pp. 1685–1694, 2018.

[28] A. Selivanov and E. Fridman, "Event-triggered H_∞ control: A switching approach," IEEE Transactions on Automatic Control, vol. 61, no. 10, pp. 3221–3226, 2016.

[29] P. Kundur, N. J. Balu, and M. G. Lauby, Power system stability and control. McGraw-hill New York, 1994, vol. 7.

[30] L. Jiang, W. Yao, Q. Wu, J. Wen, and S. Cheng, "Delay-dependent stability for load frequency control with constant and time-varying delays," IEEE Transactions on Power systems, vol. 27, no. 2, pp. 932–941, 2011.

[31] E. Weitenberg, Y. Jiang, C. Zhao, E. Mallada, C. De Persis, and F. Dörfler, "Robust decentralized secondary frequency control in power systems: Merits and tradeoffs," IEEE Transactions on Automatic Control, vol. 64, no. 10, pp. 3967–3982, Oct 2019.

[32] K. J. Åström, T. Hägglund, and K. J. Astrom, Advanced PID control. ISA-The Instrumentation, Systems, and Automation Society Research Triangle, 2006, vol. 461.

[33] A. Selivanov and E. Fridman, "A switching approach to event-triggered control," in 2015 54th IEEE Conference on Decision and Control (CDC). IEEE, 2015, pp. 5468–5473.

[34] C. Peng, J. Zhang, and H. Yan, "Adaptive event-triggering H_∞ load frequency control for network-based power systems," IEEE Transactions on Industrial Electronics, vol. 65, no. 2, pp. 1685–1694, 2017.

[35] J. Löfberg, "YALMIP: A toolbox for modeling and optimization in matlab," in Proceedings of the CACSD Conference, vol. 3. Taipei, Taiwan, 2004.

[36] K.-C. Toh, M. J. Todd, and R. H. Tütüncü, "On the implementation and usage of SDPT3–a matlab software package for semidefinite-quadratic-linear programming, version 4.0," in Handbook on semidefinite, conic and polynomial optimization. Springer, 2012, pp. 715–754.

[37] K. Vrdoljak, N. Perić, and I. Petrović, "Sliding mode based load-frequency control in power systems," Electric Power Systems Research, vol. 80, no. 5, pp. 514–527, 2010.

[38] J. Hu, J. Cao, J. M. Guerrero, T. Yong, and J. Yu, "Improving frequency stability based on distributed control of multiple load aggregators," IEEE Transactions on Smart Grid, vol. 8, no. 4, pp. 1553–1567, 2015.

Appendix
Proof of Theorem III.1

The proof is based on [33, Theorem 2]. For stability analysis of system (17), we consider the following LKF:

$$\mathcal{V} = \sum_{i=0}^{4} \mathcal{V}_i \tag{25}$$

where $x_t(\mu) = x(t+\mu)$ for $\mu \in [-h, 0]$,

$$\begin{aligned}
\mathcal{V}_0(t, x_t) &= x^T(t)Px(t),\\
\mathcal{V}_1(t, x_t) &= \int_{t-\theta_M}^{t} e^{2\alpha(s-t)} x^T(s)S_0x(s)ds,\\
\mathcal{V}_2(t, x_t) &= \theta_M \int_{-\theta_M}^{0}\int_{t+\mu}^{t} e^{2\alpha(s-t)} \dot{x}^T(s)R_0\dot{x}(s)ds d\mu,\\
\mathcal{V}_3(t, x_t) &= \int_{t-\tau_M}^{t-\theta_M} e^{2\alpha(s-t)} x^T(s)S_1x(s)ds,\\
\mathcal{V}_4(t, x_t) &= h\int_{-\tau_M}^{-\theta_M}\int_{t+\mu}^{t} e^{2\alpha(s-t)} \dot{x}^T(s)R_1\dot{x}(s)ds d\mu.
\end{aligned}$$

On differentiating $\mathcal{V}$ we get $\dot{\mathcal{V}}_0 = 2x^T(t)P\dot{x}(t)$, and

$$\begin{aligned}
\dot{\mathcal{V}}_1 =& -2\alpha\mathcal{V}_1 + x^T(t)S_0x(t) - e^{2\alpha\theta_M}x^T(t-\theta_M)S_0x(t-\theta_M)\\
\dot{\mathcal{V}}_2 =& -2\alpha\mathcal{V}_2 + \theta_M^2\dot{x}^T(t)R_0\dot{x}(t)\\
&- \theta_M\int_{t-\tau_M}^{t} e^{2\alpha(s-t)}\dot{x}^T(s)R_0\dot{x}(s)ds\\
\dot{\mathcal{V}}_3 =& -2\alpha\mathcal{V}_3 + e^{-2\alpha\theta_M}x^T(t-\theta_M)S_1x(t-\theta_M)\\
&- e^{2\alpha\tau_M}x^T(t-\tau_M)S_1x(t-\tau_M)\\
\dot{\mathcal{V}}_4 =& -2\alpha\mathcal{V}_4 + h^2\dot{x}^T(t)R_1\dot{x}(t)ds\\
&- h\int_{t-\tau_M}^{t-\theta_M} e^{2\alpha(s-t)}\dot{x}^T(s)R_1\dot{x}(s)ds.
\end{aligned} \tag{26}$$

Case (i): When $\Upsilon(t) = 0,\ \bar{\theta}(t) \in [0, \theta_M]$

$$\begin{aligned}
\dot{\mathcal{V}}_0 =& 2x^T(t)P[Ax(t) + F\Delta P_d + BKC_2x(t-\bar{\theta}(t))\\
&+ BKDv(t-\bar{\theta}(t)) + BKe(t)].
\end{aligned} \tag{27}$$

We apply Park's theorem [11, Lemma 3.4] and Jensen's inequality [11, Proposition 3.11] to compensate the term $x(t-\bar{\theta}(t))$, that is

$$\begin{aligned}
-\theta_M\int_{t-\theta_M}^{t} e^{2\alpha(s-t)}\dot{x}^T(s)R_0\dot{x}(s)ds \le e^{2\alpha\theta_M}\\
\times\begin{bmatrix} x(t)-x(t-\bar{\theta}(t)) \\ x(t-\bar{\theta}(t))-x(t-\theta_M)\end{bmatrix}^T\begin{bmatrix} R_0 & G_0 \\ G_0^T & R_0\end{bmatrix}\\
\times\begin{bmatrix} x(t)-x(t-\bar{\theta}(t)) \\ x(t-\bar{\theta}(t))-x(t-\theta_M)\end{bmatrix}
\end{aligned} \tag{28}$$

$$\begin{aligned}
-h\int_{t-\tau_M}^{t-\theta_M} e^{2\alpha(s-t)}\dot{x}^T(s)R_1\dot{x}(s)ds \le -e^{-2\alpha\tau_M}\\
\times[x(t-\theta_M)-x(t-\tau_M)]^TR_1[x(t-\theta_M)-x(t-\tau_M)].
\end{aligned} \tag{29}$$

Now consider (14) which implies

$$\begin{aligned}
0 \le \epsilon[C_2x(t-\bar{\theta}(t)) + Dv(t-\bar{\theta}(t))]\Omega\\
\times[C_2x(t-\bar{\theta}(t)) + Dv(t-\bar{\theta}(t))] - e^T(t)\Omega e(t).
\end{aligned} \tag{30}$$

Adding (26), (27), (30) and using (28), (29) we get

$$\begin{aligned}
\dot{\mathcal{V}} + 2\alpha\mathcal{V} + z^Tz - \gamma^2[\Delta P_d^T\Delta P_d + v^T(t-\bar{\theta}(t))v(t-\bar{\theta}(t))]\\
\le \eta^T(t)\tilde{\Lambda}\eta(t) + \dot{x}^T(t)(\theta_M^2R_0 + h^2R_1)\dot{x}(t)
\end{aligned}$$

where $\eta(t) = \text{col}\{x(t), x(t-\theta_M), x(t-\tau_M), x(t-\bar{\theta}), e(t), \Delta P_d(t), v(t-\bar{\theta}(t))\}$ and the matrix $\tilde{\Lambda}$ is obtained from Λ by removing the last block-column and the block-row. Substituting expression for $\dot{x}$ and employing Schur complement formula, we obtain that $\Lambda \le 0$ and therefore

$$\dot{\mathcal{V}} + 2\alpha\mathcal{V} + z^Tz - \gamma^2[\Delta P_d^T\Delta P_d + v^T(t-\tau(t))v(t-\tau(t))] \le 0. \tag{31}$$

0885-8950 (c) 2020 IEEE. Personal use is permitted, but republication/redistribution requires IEEE permission. See http://www.ieee.org/publications_standards/publications/rights/index.html for more information.
Authorized licensed use limited to: TEL AVIV UNIVERSITY. Downloaded on June 06,2020 at 10:31:27 UTC from IEEE Xplore. Restrictions apply.

This article has been accepted for publication in a future issue of this journal, but has not been fully edited. Content may change prior to final publication. Citation information: DOI 10.1109/TPWRS.2020.2999488, IEEE Transactions on Power Systems

Case (ii): When $\Upsilon(t) = 1, \tau(t) \in [\theta_M, \tau_M]$

For system (17) with $\tau(t) \in [\theta_M, \tau_M]$, we have

$$\begin{aligned}\mathcal{V}_0 =& 2x^T(t)P[Ax(t) + F\Delta P_d + BKC_2x(t-\tau(t)) \\ &+ BKDv(t-\tau(t))].\end{aligned} \tag{32}$$

To compensate for $x(t-\tau(t))$ with $\tau(t) \in [\theta_M, \tau_M]$, we apply Jensen's inequality and Park's theorem to obtain

$$\begin{aligned}-\theta_M \int_{t-\eta_m}^{t} e^{2\alpha(s-t)}\dot{x}^T(s)R_0\dot{x}(s)ds \leq -e^{-2\alpha\theta_M} \\ \times[x(t) - x(t-\theta_M)]^T R_0[x(t) - x(t-\theta_M)]\end{aligned} \tag{33}$$

$$\begin{aligned}-h\int_{t-\tau_M}^{t-\theta_M} e^{2\alpha(s-t)}\dot{x}^T(s)R_1\dot{x}(s)ds \leq e^{2\alpha\tau_M} \\ \times \begin{bmatrix} x(t-\theta_M) - x(t-\tau(t)) \\ x(t-\tau(t)) - x(t-\tau_M)\end{bmatrix}^T \begin{bmatrix} R_1 & G_1 \\ G_1^T & R_1\end{bmatrix} \\ \times \begin{bmatrix} x(t-\theta_M) - x(t-\tau(t)) \\ x(t-\tau(t)) - x(t-\tau_M)\end{bmatrix}.\end{aligned} \tag{34}$$

On adding (26), (32), and employing (33)), (34) we get

$$\begin{aligned}\dot{\mathcal{V}} + 2\alpha\mathcal{V} + z^Tz - \gamma^2[\Delta P_d^T\Delta P_d + v^T(t-\tau(t))v(t-\tau(t))] \\ \leq \kappa^T\tilde{\Gamma}\kappa + \dot{x}^T(\theta_M^2R_0 + h^2R_1)\dot{x}.\end{aligned}$$

where $\kappa(t) = \text{col}\{x(t), x(t-\theta_M), x(t-\tau_M), x(t-\tau(t)), \Delta P_d(t), v(t-\tau(t))\}$ and the matrix $\tilde{\Gamma}$ is obtained from Γ by removing the last block-column and the block-row. Substituting expression for $\dot{x}$ and z and employing Schur complement formula, we obtain that $\Gamma \leq 0$ and thus guarantees (31).

If $\Delta P_d \equiv 0$, $v \equiv 0$ then from (31), we have $\dot{\mathcal{V}} \leq -2\alpha\mathcal{V}$. Therefore the system (17) is internally exponentially stable with decay rate α and by integrating (17) from 0 to ∞ with initial condition $x(0) = 0$ we get (18).

0885-8950 (c) 2020 IEEE. Personal use is permitted, but republication/redistribution requires IEEE permission. See http://www.ieee.org/publications_standards/publications/rights/index.html for more information.
Authorized licensed use limited to: TEL AVIV UNIVERSITY. Downloaded on June 06,2020 at 10:31:27 UTC from IEEE Xplore. Restrictions apply.